Detection of High-Impedance Faults in Power Distribution Systems

Daqing Hou
Schweitzer Engineering Laboratories, Inc.

Detection of High-Impedance Faults in Power Distribution Systems

Daqing Hou, *Schweitzer Engineering Laboratories, Inc.*

Abstract—When overhead power lines in solid or low-impedance grounded systems lose supports and fall on poorly conductive surfaces, they generate high-impedance faults (HIFs). These faults are a great public safety concern because the fault currents are generally too small for detection by conventional overcurrent relays. This concern has generated great interest in the detection of downed conductor-related HIFs at the substation level. In this paper, we present an HIF detection algorithm that uses traditional relay logic. The algorithm is easier to understand and simpler to implement than many black-box detection methods such as neural networks. We discuss such key aspects of algorithm design as input quantity selection, generation of a reliable reference, adaptation to feeder ambient load noises, and decision logic based on trending and memories. We use real-world data collected from staged HIF tests and noisy substation loads to validate detection results.

I. INTRODUCTION

In power distribution systems with voltages ranging from 4 kV to 34.5 kV, high-impedance faults (HIFs) have challenged utilities and researchers for years. HIFs are those faults on distribution feeders with fault currents below traditional overcurrent relay pickups. Fallen power conductors on poorly conductive surfaces, tree branches brushing against power lines, and dirty insulators are all potential causes of HIFs. Researchers in many studies of staged HIFs on grounded distribution systems have recorded fault current magnitudes that vary anywhere from zero to less than 100 amperes.

HIFs have such small fault currents that they generally do not affect power distribution system operation. However, HIFs caused by downed power conductors are major public safety concerns. Without timely correction, these faults can be hazardous to human lives and property. There have been a number of documented cases of costly litigation as a result of damages from undetected downed power conductors.

HIFs on multigrounded distribution systems are difficult to detect at the substation level. Single-phase loads and the multipath returns of unbalanced currents are several factors contributing to the difficulty in detecting these faults [1]. A grounded system can be quite unbalanced when a major single-phase lateral is out of service. Beyond ensuring coordination with downstream devices and fuses and avoiding pickup on cold loads and transformer inrushes, one must avoid false tripping by setting conventional ground overcurrent protection above the maximum foreseeable unbalance. Thus, overcurrent protections that use the fundamental component or root-mean-square (rms) of currents are ineffective in detecting HIFs. Some HIFs, such as those resulting from downed power conductors on asphalt or dry sand, generate virtually no fault current. No substation-based devices can detect these HIFs or

down-conductor situations. An early IEEE Power Engineering Society (PES) publication [2] documented specifics on why fallen power lines cannot always be detected.

HIFs are random and dynamic. A downed power conductor can lie idle on a surface for some time and then conduct once insulation breaks down. An arcing conductor may not lie still on a ground surface, but may move around as a result of electromagnetic force. Fault current magnitudes and contents change as ground surface moisture escapes from fault-generated heat, and/or as ground silicon materials burn into glasses. Soils during different seasons of a year and from different geological regions also produce different fault current contents.

Despite these challenges, researchers remain optimistic that they will find a cost-effective substation-based detection algorithm for HIFs. Perplexed by undetected breakdowns of cross-linked polyethylene (XLP)-covered conductors in the early 1970s, Pennsylvania Power and Light Company (PP&L) initiated several staged HIF tests by dropping XLP conductors on different ground surfaces [3]. EPRI and CEA directed research in the late 1970s and early 1980s that resulted in several research reports [4]–[7]. Since then, researchers have studied and applied many existing and emerging techniques to HIF detection. These include statistical hypothesis tests [8], inductive reasoning and expert systems [9], neural networks [10] [11], third harmonic angle of fault currents [12], wavelet decomposition [13] [14], decision trees [15], fuzzy logic [16], and others. The IEEE PES and Power System Relaying Committee (PSRC) have followed the developments closely and have offered a tutorial course [17] and published committee reports [18]–[20].

As indicated by a lengthy history of on-going research and the number of technologies researchers have studied and applied, one can obtain a sense of the difficulty and complexity involved in designing an HIF detection algorithm that is both fairly dependable and 100 percent secure against false alarms.

While it is relatively easy to design an algorithm that detects certain HIFs, it is challenging to make the same algorithm secure. The objective of HIF protection is to remove hazards to the public. When an HIF detection device indicates a fault, utilities must make tripping decisions based on a number of circumstances to ensure a trip will not cause more hazardous situations. Utilities cannot tolerate false alarms from HIF detection devices. It can be more dangerous and costly, for example, to trip out a busy traffic intersection, hospital, or an airport load.

In this paper, we present another HIF detection algorithm. In Section II, we identify and introduce the key areas of de-

signing effective detection algorithms. These include input quantity selection, generation of a reliable reference, adaptation to individual feeder ambient conditions, a trending and memory function, and decision logic that uses simple, traditional relay logics. In Section III, we present the test results we obtained with the algorithm, using data from staged HIF tests. We also verify algorithm security through the use of representative noisy substation loads.

II. DESIGN OF HIGH-IMPEDANCE DETECTION

From our research and study of the subject, we identify the following as key elements to successful design of an HIF detection algorithm:

- An informative quantity that reveals HIF signatures as much as possible without being affected by loads and other system operation conditions.
- A running average of the quantity that provides a stable prefault reference. The average is preferably available at all times, even during an HIF condition. For this purpose, the running average must not follow the large fault quantity quickly during a fault event.
- An adaptive tuning feature that learns and tunes out feeder ambient noise conditions. Preferably, the tuning is active whenever the algorithm does not detect an HIF condition on the system.
- An effective decision logic to differentiate an HIF condition from other system conditions such as switching operations and noisy loads.

The HIF detection algorithm we propose centers on these key elements but contains other supplementary function blocks. Fig. 1 shows the block diagram of the algorithm for the A-phase current. The same processing also applies to the B-phase, C-phase, and residual currents.
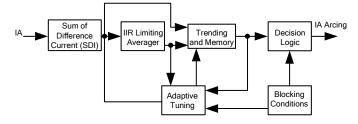

Fig. 1.   Block diagram of high-impedance detection

The first function block calculates a signal quantity upon which the algorithm bases its HIF detection. This quantity is called the Sum of Difference Current, or SDI. An Infinite-Impulse-Response (IIR) Limiting Averager establishes a stable reference for SDI. The Trending and Memory block compares SDI with the SDI average and memorizes the time and a ratio if SDI is a set threshold above the SDI average. The Decision Logic uses the results from the Trending and Memory block to determine the existence of HIF on the processed phase. The Adaptive Tuning block monitors feeder background noise during normal system operations and establishes a comparison threshold for the Trending and Memory block.

The IIR Limiting Averager also uses this threshold to prevent the averager input magnitude from becoming too large.

The following text provides details of major functions in Fig. 1.

A. Sum of Difference Current (SDI)

Because HIFs generated low current magnitudes, people realized from the beginning that they would have to search for signal quantities other than the rms and fundamental frequency component of currents for HIF detection.

HIFs typically involve arcing and conduction through ground surfaces. Both arcing and soil conduction present nonlinear resistance to current flow and therefore generate harmonics [4]. On the other hand, normal nonlinear loads such as motor centers, power inverters, and arc furnaces also generate significant harmonics, especially odd harmonics. What we want are signal quantities that reveal mostly the signatures of HIFs but vanish under normal system operation conditions.

Initially, people used the sequence components of the fundamental frequency, third and fifth harmonics, third-harmonic phase and magnitude changes, and high-frequency components between 2 kHz to 10 kHz [5]–[7]. Each of the components has its mysteries and limits. Eventually, people discussed and applied such large types of signals as current differences [11] [22], even, odd and nonharmonics [9], and energies of special frequency bands from wavelet decomposition [13] [14]. One reference [21] has suggested using the combination of different signals.

In our design, we chose to use an SDI, shown in Fig. 2, as the fault detection input. The system tracks power system frequency and samples feeder currents (I_k) at an integer number (Nspc) of samples per system cycle. The system uses a simple one-cycle difference filter [22] to calculate difference current (DI_k) and obtains SDI by accumulating the absolute values of the difference current during several power cycles (Ns).
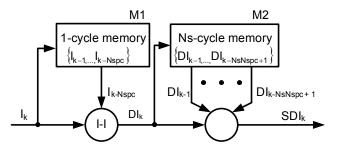

Fig. 2.   Calculation of Sum of Difference Current (SDI)

Fig. 3 illustrates the SDI calculation in time domain with the current waveform from an HIF sampled at 32 samples per Icycle. For ideal sinusoidal waveforms, the one-cycle difference calculation would result in an output of all zero values. With the arcing current of an HIF, however, the one-cycle difference of the current reveals the activity of the rather random arcing process.
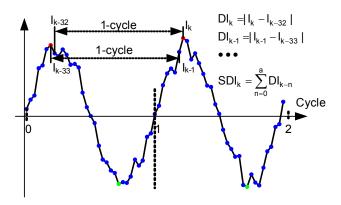
Fig. 3. Time domain illustration of SDI calculation

Fig. 4 shows the magnitude portion of the frequency response of the one-cycle difference calculation to the fourth harmonic. Note that the magnitude response has a zero at every harmonic frequency, and that this includes the dc and the fundamental frequency. All harmonic components, including the dc and the fundamental of the current, are therefore removed after the difference calculation. The frequency contents of the difference current contain only nonharmonics. SDI represents an average measure of the total nonharmonic content of a current over an Ns-cycle window, making SDI a valuable tool for HIF detection.
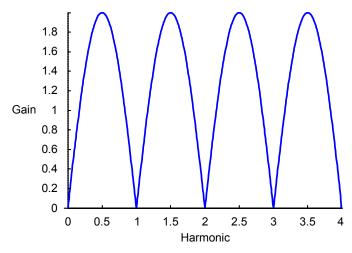

Fig. 4. Frequency magnitude response of the one-cycle difference filter

B. IIR Limiting Averager

When an HIF occurs, the SDI quantity increases. The amount of increase can be appreciated only by comparing the quantity with its history. Providing a reliable reference is the function of the IIR Limiting Averager, and the quality of this reference is important to the success of the detection algorithm.

We chose to use an infinite-impulse-response (IIR) type of averaging with a fixed time constant, because we can achieve long-time memory effects efficiently with relatively few calculations and memory units. One must choose a time constant large enough to provide a stable reference during faults. On the other hand, a small time constant is good for allowing a rapid tracking of the input average during no fault conditions. To strike a balance between these conflicting requirements

and to prevent the average from following quickly the large SDI spikes, the input to the averager is limited when the SDI value is above a threshold. One other possibility for stabilizing the average output in case of high input spikes is to increase the time constant. Some distance relays use this method, described in US patent 5,790,418 [23] in the memory filter for the polarizing quantity.

Fig. 5 shows the details of the IIR Input Limiting Averager. The averager output, SDI_REF_k, follows the general first order IIR equation (1)

$$SDI\_REF_k = (1-\alpha) \bullet x_{in} + \alpha \bullet SDI\_REF_{k-1} \qquad (1)$$

where α relates to the time constant and x_{in} can take two possible values according to the output of comparator C1. The input to the positive polarity of the comparator C1 is SDI_k, and the input to the negative polarity of the comparator C1 is $G_{IIR1}d + SDI\_REF_{k-1}$. The Adaptive Tuning section introduces the variable d. Treat this variable here as a constant. The comparator output is a logical 1 if $SDI_k > G_{IIR1}d + SDI\_REF_{k-1}$, and a logical 0 otherwise. When the comparator output is a logical 0, the switch SW is in its position 1 and x_{in} therefore equals SDI_k. When the comparator output is a logical 1, the switch SW is in its position 2 and x_{in} therefore equals $G_{IIR2}d + SDI\_REF_{k-1}$. We can then calculate the averager output, SDI_REF_k, from (2).

$$\text{if} \quad SDI_k < G_{IIR1} \bullet d + SDI\_REF_{k-1}$$

$$\text{then} \quad SDI\_REF_k = (1-\alpha) \bullet SDI_k + \alpha \bullet SDI\_REF_{k-1} \quad (2)$$

$$\text{otherwise} \quad = (1-\alpha) \bullet G_{IIR2} \bullet d + SDI\_REF_{k-1}$$
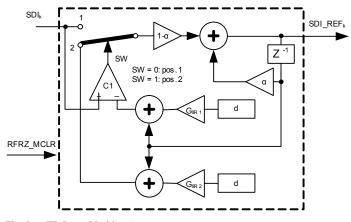

Fig. 5. IIR Input Limiting Averager

When conditions other than HIFs occur, the freeze input, RFRZ_MCLR, is a logical 1 and the IIR limiting average calculation is suspended. These non-HIF conditions include large changes in phase currents and changes in line voltages.

C. Trending and Memory

Once the algorithm establishes detection quantity SDI and its average SDI_REF, the algorithm must extract HIF signatures from these quantities. The Trending and Memory function records unusual SDI changes related to system HIF and memorize these changes for the decision logic. The Trending and Memory function provides information regarding how

often and by how much SDI departs from SDI_REF plus a margin.

Fig. 6 shows the details of the Trending and Memory function. The part of the logic before the comparator C runs at the rate of every SDI update. The remaining portion of the logic runs whenever the output of C is a logical 1.
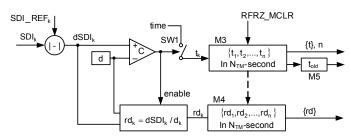

Fig. 6.   Trending and Memory function

The absolute value of the difference between SDI and SDI_REF, or dSDI, goes to the positive input of the comparator C. The negative input of the comparator connects to a variable d. The Adaptive Tuning section introduces variable d.

When dSDI exceeds d, the comparator output is a logical 1, Otherwise, the comparator output is a logical 0. A logical 1 from comparator C closes the switch SW1, and the algorithm records in a memory, M3, the time at which SW1 closes. This memory has enough units to save the maximum possible number of t_k within N_{TM} seconds.

At the beginning of each N_{TM}-second segment, if previous set $\{t_1, t_2, …, t_n\}$ is not zero, the last time value, t_n, moves to a single memory unit, M5, as t_{old}. If the set $\{t_1, t_2, …, t_n\}$ has no members, M5 retains its previous value as t_{old}.
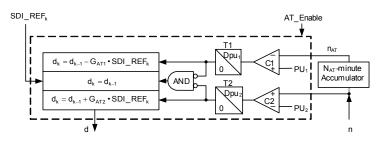
The Trending and Memory function provides $\{t\}$, $\{rd\}$, and $t_{old,}$ to the decision logic to determine the existence of an HIF. The function also provides the value n, the number of times SDI departs from the threshold of SDI_REF plus d in previous N_{TM} seconds, to the adaptive tuning logic. The algorithm uses the same blocking conditions as those in the IIR Limiting Averager, RFRZ_MCLR, for this Trending and Memory function to clear memorized $\{t\}$ and $\{rd\}$ in case of system conditions other than HIFs.
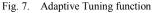
D. Adaptive Tuning

When setting traditional overcurrent relays, one uses a short circuit study program to calculate the fault current under different system operation conditions. The fault current satisfies Ohm's law, so the settings calculation process is straightforward with known system topologies and parameters.

For HIF detection, however, the situation is different. HIF detection uses nontraditional quantities. Nonlinear and dynamic feeder loads influence these quantities in different ways. For example, if the HIF detection algorithm uses the fifth harmonic of currents, detection settings would be different for feeders with six-pole power inverters than for feeders that have only relatively quiet residential loads. Given the vast variety of distribution loads, it would be impractical for users to study the loads of each feeder and determine the effects these loads have on the detection algorithm they choose to use.

The purpose of the Adaptive Tuning function is for the algorithm to automatically characterize the detection quantity of a feeder for its normal loads. The function learns a margin above the SDI average into which the SDI value may fall as a result of normal system operations. Both the IIR Limiting Averager and Trending and Memory functions use this margin, labeled as variable d.

Fig. 7 shows details of the Adaptive Tuning function. There are two inputs, n and n_{AT}, on the right side of Fig. 7. The input, n, is the number of times that SDI departed its average plus the margin d within the previous N_{TM} seconds, as this paper explained previously. An accumulator adds all n values for as long as N_{AT} minutes and produces an output n_{AT}, the number of times that SDI departs its average plus the margin d within the previous N_{AT} minutes.

Fig. 7.   Adaptive Tuning function

The first comparator of the logic, C1, compares the value of n_{AT} to a threshold PU_1. If n_{AT} is less than PU_1, the output of C1 is a logical 1. Otherwise, the output of C1 is a logical 0. If the output of comparator C1 is logical 1 for a consecutive period of D_{pu1} minutes, as the timer T1 determines, the timer T1 produces an output of logical 1. This logical 1 output enables the upper row d update calculation and at the same time causes the AND gate to force its output to a logical 0. In other words, if SDI does not depart its average plus a margin d for more than PU_2 times for D_{pu1} minutes, the algorithm considers the margin d too large and decreases the corresponding update calculation by G_{AT1} percent of the average, as in (3).

$$d_k = d_k - G_{AT1} \cdot SDI\_REF_k \qquad (3)$$

The second comparator of the logic, C2, compares the value of n to a pickup threshold PU_2. If n is greater than PU_2, the output of C2 is a logical 1. Otherwise, the output of C2 is a logical 0. If the output of comparator C2 is a logical 1 for a consecutive period of D_{pu2} seconds, as the timer T2 determines, the timer T2 produces an output of logical 1. This logical 1 output enables the bottom row d update calculation and at the same time causes the AND gate to force its output to a logical 0. In other words, if SDI departs its average plus a margin d for more than PU_2 times in N_{TM} seconds, and if the condition lasts for D_{pu2} seconds, the algorithm considers the margin d too small and increases the corresponding update calculation by G_{AT2} percent of the average, as in (4).

$$d_k = d_k + G_{AT2} \cdot SDI\_REF_k \qquad (4)$$

If both outputs of T1 and T2 are logical 0, the AND gate produces a logical 1 output, which enables the middle row

update calculation for d. The new d value does not differ from the previous value.

The enable input of Fig. 7, AT_Enable, determines when the d update occurs. Some distribution loads, such as a rail train system, have daily cycles, and other loads such as motor pumps for farms have seasonal cycles. Ideally, the tuning process should be continuous as long as there are no HIFs on the system. The tuning should also remain for a certain period of time after a breaker closure and load current detection.

E. Decision Logic

The Trending and Memory function provides rich information regarding how often and by how much SDI departs from its reference plus a learned margin. The value of n represents the number of times SDI departed its threshold within the previous N_{TM} seconds, while the set of ratios, $\{rd\}$, represents the information concerning the amount by which SDI exceeded its threshold. The first block of the decision logic in Fig. 8 calculates a set of time differences, $\{dt\}$, through the use of the set of time, $\{t\}$, and t_{old} from the Trending and Memory function. The time difference can provide the temporal characteristic of randomness signature of the HIFs. It is possible to use some artificial intelligence methods of classification and pattern recognition, such as neural network or decision trees, to decipher this information for the detection of HIFs. We chose, instead, to use relatively simple comparators and counters for the decision logic.
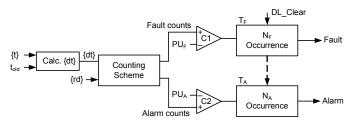

Fig. 8.   Block diagram of decision logic

The decision logic has two counters for separate HIF alarms and trip. Counter T_F is for HIF detection, and Counter T_A is for HIF alarms. For each pair of $\{rd,dt\}$ in the previous N_{TM}-second segment, a counting scheme determines whether to count or not count and the number of counts for a fault or alarm. For each N_{TM}-second segment, if the number of counts for an HIF exceeds PU_F, as comparator C1 determines, the comparator produces a logical 1 output. Counter T_F accumulates the number of logical 1 assertions from comparator C1. If N_F occurrences accumulate within a fault decision time, counter T_F produces a logical 1 output to indicate detection of an HIF. The algorithm uses a similar method for deriving an alarm for an HIF through comparator C2 and counter T_A, but it uses different detection thresholds, as Fig. 8 indicates.

Fig. 9 shows an rd-dt plane. The entire plane is divided into three regions: Fault Count, Alarm Count, and No Count. The dt axis has a unit of Ns-cycle, the interval over which SDI accumulates. If a $\{rd,dt\}$ pair falls into the no-count region, the algorithm generates no counts for either alarm or fault. If a $\{rd,dt\}$ pair falls into the alarm-count region, the algorithm generates counts only for HIF alarms. If a $\{rd,dt\}$ pair falls

into the fault-count region, the algorithm generates counts for both fault and alarm conditions of HIFs.
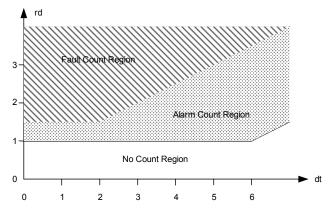

Fig. 9.   Counting regions for alarm and fault conditions

This counting scheme on the rd-dt plane is much like the percentage restraint current differential characteristic, with dt similar to the restraining quantity and rd similar to the operating quantity. Sporadic and isolated high SDI values can arise from system switching such as turning capacitor banks on and off or moving load tap changers up and down. Such values can also result from lightning strikes during storm seasons. We can discount these SDI events because they are associated with large dt values. On the other hand, intense and active arcing events from HIFs tend to produce high SDI values clustered in a short period of time, so the related $\{rd,dt\}$ pairs would be more likely to reside in the operating region of the counting scheme.

Fig. 10 shows how the algorithm generates the number of counts as a function of the ratio, rd, for each $\{rd,dt\}$ pair that the counting scheme shown in Fig. 9 determines to be countable. For example, if the rd value in a $\{rd,dt\}$ pair is 4, and the pair falls into the Fault Count region, then the algorithm generates not one but two fault and alarm counts for this pair of $\{rd,dt\}$. Studies of staged HIF data indicate that the SDI value generally correlates to the relevance of an event to HIFs. By making the number of counts proportional to the ratio, rd, the algorithm considers not only the event that SDI overcomes its threshold, but also the amount of SDI increase, in determining the existence of a fault.
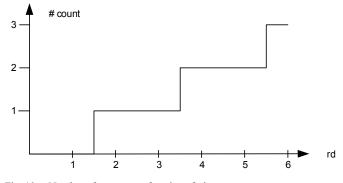

Fig. 10.   Number of counts as a function of rd

Several system conditions disable the decision logic as indicated by the DL_Clear input. Some of these conditions include large phase current and some voltage changes. The algo-

rithm also detects and uses events that occur in all three phases to disable the decision logic, because we assume that these events are highly unlikely HIFs.

III. SIMULATION TEST WITH STAGED FAULT AND SUBSTATION LOAD DATA

A. High-Impedance Fault Simulation

In early HIF studies, researchers performed and recorded many staged faults [6] [7]. Test data from these studies have provided valuable information toward understanding and characterizing HIFs. These data provided the foundation for the design of many early detection devices.

Over time, researchers constructed various HIF models for the purpose of designing and testing fault detection algorithms. These models ranged from simple diodes and dc sources connected in series to variable resistances that one could control through the relationship between the voltage and current of some typical HIFs [24].

Nevertheless, HIFs are complicated processes that include many nondeterministic variables yet to be understood. As reference [25] explains, the impedance of these faults includes those of arcs, ground surface, earth return, and the interface between ground surfaces and downed conductors. Researchers have conducted extensive studies on some impedance, such as that of arc, but the results probably cannot be applied directly in HIF situations because of the voltage level, length of arc, and multiple paths of arc. Some other impedance such as that of earth return has a well-established formula; but it is difficult to determine some necessary parameters used in the formulation. Many other variables, such as conductor types, the way a conductor contacts the ground surface, surface types, ground moisture content, and return earth compositions, can all change in too many ways to be accurately accounted for in simulations.

It is therefore our belief that HIF simulations can provide initial data for preliminary research, but ultimate fault detection algorithm design and verification should rely on staged fault tests that cover fairly broad geographical terrains, climates, and ground surface types.

B. Data Acquisition Device

To prepare for staged fault test data collection, we assembled two identical data acquisition systems. The data acquisition devices we used are Daqbook/2005® devices from IOtech. These devices can sample as many as 16 analog channels at a sampling frequency as great as 20 kHz. The Daqbook/2005 device communicates with computers through an Ethernet port and saves acquired data directly onto the computers. To interface with Daqbook/2005 devices, we made signal interface modules that include CT/PT and analog low-pass filter circuitries typical of microprocessor relays. The cutoff frequency of a two-stage RC low-pass filter is at about 5.8 kHz. We also used a wireless router in the system to provide isolation between the personal computer and the substation secondary circuits. The router also allows flexible placement of a data acquisition device in a substation and test site. As the field setup photo in Fig. 11 shows, every component of the system fits in a briefcase.
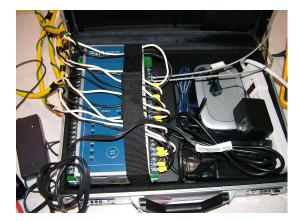

Fig. 11.   Data acquisition device used in staged high-impedance fault tests

C. Staged High-Impedance Fault Tests

We staged four HIF tests at three different locations in 2005. In all tests, we collected voltages and currents at both the test site and the substation. Test site data allow us to study the way that HIF signatures propagate back to the substation. We use the substation data for detection algorithm design and test.

The first test was on Feeder 1503 from the South Nacogdoches substation of TXU Electric Delivery. This is a 138 kV/12.5 kV substation. We staged the HIFs at two different locations on the feeder. One site was about 2 miles from the substation, and the other site was 12.7 miles from the substation. The ground surfaces we used in both tests included concrete blocks, grassy earth, dry and wet gravels, dry and wet sands, asphalt, tree limbs, and a car tire. At the end of the tests, we also turned on and off two feeder capacitor banks and raised and lowered the tap of a transformer load-tap changer to record normal system switching events.

Fig. 12(a) and Fig. 12(b) show the currents of a TXU earth fault at the test site and the substation, respectively. The time scales of the two plots are not synchronized. We staged the fault by dropping a conductor on dampened, grassy earth. The peak fault current of about 30 amperes shows quite clearly in the substation measurement.
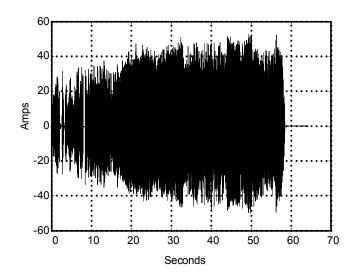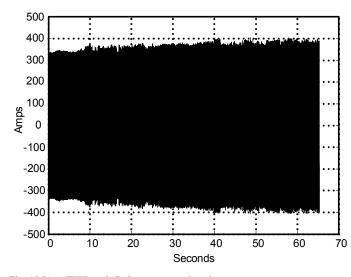
Fig. 12(a).   TXU earth fault current at test site

Fig. 13(a).   IPC gravel/earth fault current at test site

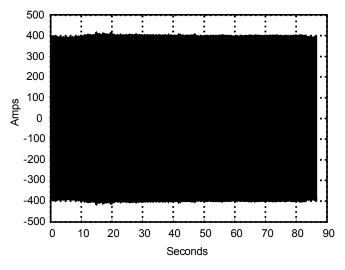Fig. 12(b).   TXU earth fault current at substation

Fig. 13(b).   IPC gravel/earth fault current at substation

The second test was on Feeder CDAL0017 from the Cloverdale 138 kv/12.5 kV substation of Idaho Power Company. The test site is about one mile from the substation. The test surfaces included a concrete block, earth, mixture of sand and gravels, dry and wet asphalt, dry and wet railroad gravel, a car tire, and maple and juniper trees.

Fig. 13(a) and Fig. 13(b) show the currents of an IPC gravel/earth fault at the test site and substation, respectively. Again, the time scales of the two plots are not synchronized. We staged the fault by dropping a conductor on a six-inch-thick mixture of gravel and dirt. It is virtually impossible to see any sign of this approximately three-ampere fault current in the substation measurement.

We staged the last two tests on Feeder 4040 from the Patzcuaro 115 kV/13.8 kV substation of CFE in central Mexico. The test location is on farmland about eight miles from the substation. We performed the first test in June of 2005, during the dry season for the area. The ground surface was fine powder dirt with some dry plant stems. We began the test by dropping a covered conductor on the dirt. We then progressed with stripping about one meter of cover off the conductor, watering the ground, and installing a one-meter ground rod. We used no protection fuse at the test site. We performed the second test in September of 2005, during the rainy season for the area, at exactly the same location. We went through a similar test sequence of dropping a covered conductor, laying a stripped bare conductor on the ground, and installing as many as three grounding rods. The fault current we obtained for the second test is generally several times larger than the current we recorded in the first test.

Fig. 14(a) and Fig. 14(b) show currents from a second CFE fault test at the test site and substation, respectively. The time scales of the two plots are not synchronized. We staged the fault by dropping a covered conductor and then forcing the tip of the conductor to touch a ground rod. The fault current is

about 10 amperes. The substation measurement shows many large changes in the current envelope that are unrelated to the fault; these changes exist also on the unfaulted phase.
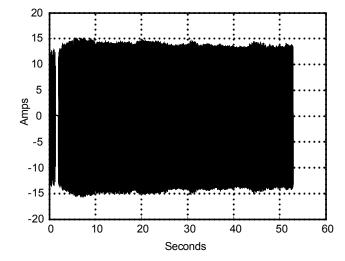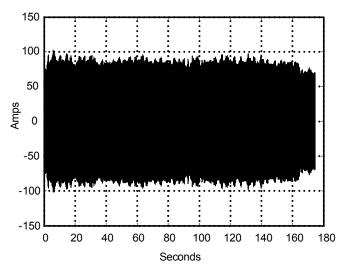

Fig. 14(a). CFE earth fault current at test site

Fig. 14(b). CFE earth fault current at substation

D. Simulation Results of Detection Algorithm

We used Matlab® programming language in a graphical user interface (GUI) setup to fully simulate the detection algorithm we described previously. We can use the setup to handle data loading, channel assignments, settings change, and selection of plot quantities. We saved all collected fault data in COMTRADE format at different sampling frequencies for further investigation. Because of the limited length of prefault data, several functions of the fault detection algorithm needed special treatments under the simulation environment. These functions included IIR Limiting Averager and Adaptive Tuning. We used a fast charge process to move the simulation process quickly into the prefault state. Through use of the COMTRADE format, we could easily extend the prefault portion of each fault event.

Fig. 15 shows the detection simulation results for the staged TXU fault event the paper illustrates in Fig. 12. The lower analog portion of the plot shows the SDI quantity for

the event. This portion of the plot also shows in a dashed line the tuned threshold plus the IIR averager output, or d + SDI_REF. Whenever SDI exceeds this threshold, the algorithm records the time and calculates a ratio, which the Trending and Memory function saves for later investigation. One can see that the SDI value increases after the fault is applied at approximately 8 seconds. Also note that the SDI shows many large spikes that are typical for HIFs. The upper portion of the plot shows four digital elements named, from bottom to top, A-SDI, B-SDI, C-SDI, and G-SDI. These are fault detection outputs for, respectively, phases A, B, C, and the residual current channel. A thick bar on the digital plot indicates a fault detection with an "F" marking the starting point of a detection. For this event, one can see that the detection algorithm is able to detect the fault correctly in the faulted B phase. The pickup in the residual channel also indicates fault detection.
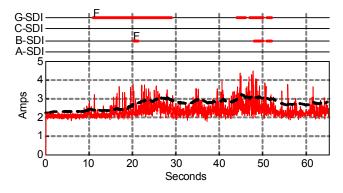

Fig. 15. Fault detection simulation results for TXU earth fault

Fig. 16 shows the detection simulation results for the IPC event the paper illustrates in Fig. 13. As we might expect because of the small fault current, the arcing activity reflected in the SDI quantity is insufficient to cause pickup of the fault detection element. It is possible to fine-tune settings to detect this fault event, but we have established overall settings to retain high security for the algorithm. Any attempt to make the detection more sensitive would inadvertently sacrifice security.
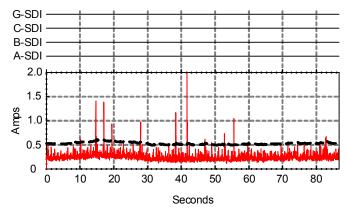

Fig. 16. Fault detection simulation results for IPC gravel/earth fault

Fig. 17 shows the detection simulation results for the CFE event the paper illustrates in Fig. 14. The strong SDI activity makes this event easy for the HIF detection algorithm to detect.
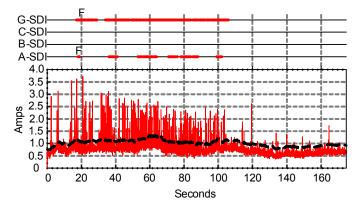
Fig. 17. Fault detection simulation results for CFE earth fault test

E. Security Test With Noisy Substation Loads

As previous studies pointed out, it is difficult to design an HIF detection algorithm that is totally immune to false alarms. It is also a great challenge to test the security aspect of a detection algorithm. Collecting all foreseeable system events or operation conditions that can cause security problems for a detection algorithm takes time and is an on-going task.

After testing the algorithm with system-switching events including such devices as capacitors and load-tap changers, we identified feeders with extremely noisy loads and collected voltages and currents from these loads for as long as 24 hours to further test the security aspect of the detection algorithm. The loads we collected included those of a cheese manufacturer, motor pumps, a foundry, car crushers, and a metropolitan rail transit system.

Fig. 18 shows the cheese manufacturer load during a five-minute period. The upper plot is the A-phase current. The bottom plot contains the total harmonic distortion in the upper trace and the SDI quantity in the lower trace. The total harmonic distortion and the SDI are shown in percentage to the fundamental frequency component. The load consists mostly of motor drives. Total harmonic distortion is close to 28 percent, of which most is fifth harmonic (26 percent) and third harmonic (8 percent). It is a very noisy load in terms of the harmonic contents. However, the load is quiet in the sense that it does not generate and change the SDI quantity that the detection algorithm uses.
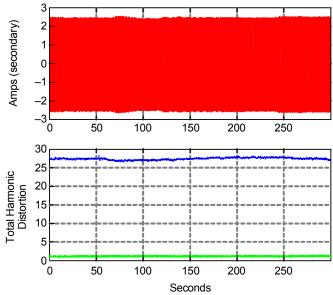

Fig. 18. Five-minute cheese manufacture load–A phase (secondary)

Fig. 19 shows in its upper plot the A-phase current of the metropolitan rail transit system load. The bottom plot shows the total harmonic distortion (upper trace) and the SDI quantity (lower trace). Although the percentage total harmonic distortion of this load is not large, the rail load is noisy in that it causes large variations in rms value, harmonic contents, and the SDI quantity of the currents. The load is not always as noisy as shown in Fig. 19. In the early morning, when the trains are not operating, the load is as quiet as typical residential and commercial loads.

The detection algorithm "learns" this load noise through the use of the adaptive tuning feature and retains its security even in such an extremely noisy load environment. HIFs must present strong fault signatures before the algorithm indicates fault detection. Because the load characteristics encroach those of HIF signatures, security is guaranteed while the dependability of fault detection is compromised.
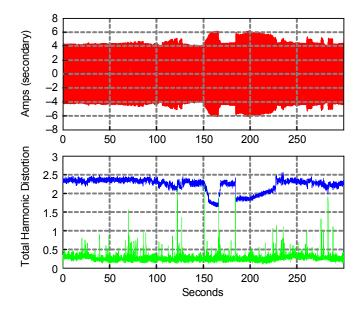

Fig. 19. Five-minute rail transportation load–A phase (secondary)

Fig. 20 shows the plots of the same quantities as those in Fig. 18 and Fig. 19 for a car crusher load during working hours. While the envelope of the A-phase current resembles those of some HIFs, its harmonic contents and the SDI quantity show few changes pertaining to HIFs. This type of load causes no detection security concern and results in no compromise in the dependability of fault detections.
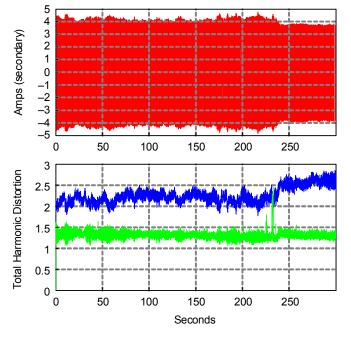

Fig. 20.   Five-minute car crusher load–A phase (secondary)

IV. Conclusions

HIFs resulting from downed conductors create public safety concerns. Depending on ground surface materials and conditions, some HIFs generate little or no fault currents. It is therefore impossible to design a substation-based detection device to detect all HIFs and downed conductor conditions.

Nevertheless, it is possible to detect many HIFs through the use of some signatures of HIFs contained in signal quantities other than current rms or fundamental frequency components.

We have introduced in this paper an HIF detection algorithm that is simple to understand and economical to implement. The algorithm uses an SDI quantity that reveals signatures of HIFs while remaining generally free of contamination by distribution loads. Through the use of an adaptive tuning process, the algorithm can "learn" the ambient noise profile of distribution feeders and therefore increase the security of fault detections. A novel IIR Limiting Averager provides a stable reference for SDI during switching and fault conditions. The detection logic uses operating and restraining quantities and counts both temporal and amplitude characteristics of an HIF.

Tests of the detection algorithm used data from real-world HIFs that included large geological regions, a wide range of climates, and many foreseeable types of ground surfaces. The algorithm has proven capabilities beyond those of traditional overcurrent relays for detecting large portions of HIFs.

Real-world data also verify the security of the algorithm. These data come from tests that include system-switching conditions and as long as 24-hour noisy feeder loads such as car crushers, foundries, rail transportation systems, and motor pumps and centers.

When a distribution feeder contains noisy loads that encroach on the signature of HIFs, the adaptive tuning function of the detection algorithm automatically tunes to enhance security. In the classical tradeoff between security and dependability, such situations cause an inadvertent negative impact on fault detection dependability.

V. Acknowledgment

VI. References

[1] D. Hou and N. Fischer, "Deterministic High-Impedance Fault Detection and Phase Selection on Ungrounded Distribution Systems," in *2005 32nd Annual Western Protective Relay Conference Proceedings*.

[2] IEEE Power Engineering Society, *Downed Power Lines: Why They Can't Always Be Detected*, New York: IEEE, 1989.

[3] PP&L, "Report of Distribution Conductor Staged Fault Tests," Oct. 1973.

[4] J. Carr, G. L. Hood, "High Impedance Fault Detection on Primary Distribution Systems," CEA Final Report, Project No. 78–75, Nov. 1979.

[5] I. Lee, "High Impedance Fault Detection Using Third Harmonic Current," EPRI Final Report, EPRI EL-2430, June 1982.

[6] S. J. Balser, K. A. Clements, E. Kallaur, "Detection of High Impedance Faults," EPRI Final Report, EPRI EL-2413, June 1982.

[7] B. D. Russell, B. M. Aucoin, T. J. Talley, "Detection of Arcing Faults on Distribution Feeders," EPRI Final Report, EPRI EL-2757, Dec. 1982.

[8] S. J. Balser, K. A. Clements, D. J. Lawrence, "A Microprocessor-Based Technique for Detection of High Impedance Faults," *IEEE Trans. Power Delivery*, vol. 3, pp. 252–258, July 1986.

[9] C. J. Kim, B. D. Russell, "Classification of Faults and Switching Events by Inductive Reasoning and Expert System Methodology," *IEEE Trans. Power Delivery*, vol.. 3, pp. 1631–1637, July 1989.

[10] S. Ebron, D. L. Lubkeman, M. White, "A Neural Network Approach to The Detection of Incipient Faults on Power Distribution Feeders," *IEEE Trans. Power Delivery*, vol. 2, pp. 905–914, April 1990.

[11] A. P. Apostolov, J. Bronfeld, C. H. M. Saylor, P. B. Snow, "An Artificial Neural Network Approach to the Detection of High Impedance Faults," in *1993 International Conference on Expert System Applications for the Electrical Power Industry Proceedings*.

[12] D. I. Jeerings, J. R. Linders, "A Practical Protective Relay For Down-Conductor Faults," *IEEE Trans. Power Delivery*, vol. 2, pp. 565–574, April 1991.

[13] J. Liang, S. Elangovan, J. B. X. Devotta, "A Wavelet Multiresolution Analysis Approach to Fault Detection and Classification in Transmission Lines," *International Journal of Electrical Power and Energy Systems*, vol. 20, Issue 5, pp. 327–332, June 1998.

[14] T. M. Lai, L. A. Snider, E. Lo, "Wavelet Transformation Based Algorithm for the Detection of Stochastic High Impedance Faults," in *Proc. International Conference on Power System Transients (IPST 2003)*, New Orleans, LA, September 2003.

[15] Y. Sheng and S. M. Rovnyak, "Decision Tree-Based Methodology For High Impedance Fault Detection," *IEEE Trans. Power Delivery*, vol. 2, pp. 533–536, April 2004.

[16] F. G. Jota and P. R. S. Jota, "High-Impedance Fault Identification Using a Fuzzy Reasoning System," *IEE Proceedings – Generation, Transmission and Distribution*, vol. 145, Issue 6, pp. 656–661, Nov. 1998.

[17] *Detection of Downed Conductors on Utility Distribution Systems*, IEEE PES Tutorial Course, 90EH0310-3-PWR, Piscataway, NJ: IEEE, 1989.

[18] "The Interruption of Downed Conductors on Low Voltage Distribution Systems," Report prepared by the IEEE Power System Relaying Committee for the Electric Power Research Institute, Oct. 1976.

[19] J. T. Tengdin, E. E. Baker, J. J. Burke, B. D. Russell, R. H. Jones, and T. E. Wiedman, "Application of High Impedance Fault Detectors: a Summary of the Panel Session Held at the 1995 IEEE PES Summer Meeting" in *Proc. Transmission and Distribution Conference*, Los Angeles, CA, Sept. 1996.

[20] "High Impedance Fault Detection Technology," Report of IEEE PSRC Working Group D15, March 1996. [Online] Available: http://grouper.ieee.org/groups/td/dist/documents/highz.pdf.

[21] H. J. Songster, "High Impedance Fault Detection," in *1980 7th Annual Western Protective Relay Conference Proceedings*.

[22] J. J. Zuercher and C. J. Tennies, "Arc Detection Using Current Variation," U.S. Patent 5,452,223, Sept. 19, 1995.

[23] J. B. Roberts and D. Hou, "Adaptive Polarizing Memory Voltage Time Constant," U.S. Patent 5,790,418, Aug. 4, 1998.

[24] S. R. Nam, J. K. Park, Y. C. Kang, and T. H. Kim, "A Modeling Method of a High Impedance Fault in a Distribution System Using Two Series Time-Varying Resistances in EMTP," in *IEEE Power Engineering Society Summer Meeting*, vol. 2, pp. 1175–1180, July 2001.

[25] D. I. Jeerings, J. R. Linders, "Ground Resistance – Revisited," *IEEE Trans. Power Delivery*, vol. 2, pp. 949–956, April 1989.

VII. Biography

Daqing Hou received B.S. and M.S. degrees in Electrical Engineering at the Northeast University, China, in 1981 and 1984, respectively. He received his Ph.D. in Electrical and Computer Engineering at Washington State University in 1991. Since 1990, he has been with Schweitzer Engineering Laboratories, Inc., Pullman, Washington, USA, where he has held numerous positions including development engineer, application engineer, and R&D manager. He is currently a principal research engineer. His work includes system modeling, simulation, and signal processing for power systems and digital protective relays. His research interests include multivariable linear systems, system identification, and signal processing. He holds multiple patents and has authored or co-authored many technical papers. He is a Senior Member of IEEE.